arXiv:1210.1957v1 [cond-mat.mes-hall] 6 Oct 2012

Robust Quantum Gates for a Singlet-Triplet Spin Qubit

Hugo Ribeiro,[1] J. R. Petta,[2,3] and Guido Burkard[1]

[1]*Department of Physics, University of Konstanz, D-78457 Konstanz, Germany*
[2]*Department of Physics, Princeton University, Princeton, New Jersey 08544, USA*
[3]*Princeton Institute for the Science and Technology of Materials (PRISM),*
Princeton University, Princeton, New Jersey 08544, USA

We show that universal quantum control of a two-electron singlet-triplet spin qubit can be achieved using Landau-Zener-Stückelberg interferometry. Going beyond normal Landau-Zener dynamics with infinitely long constant velocity sweeps across an energy level anti-crossing, we focus on a physical system consisting of a two-electron double quantum dot, where the spin states can be admixtures of charge states and the level velocity can be tuned in a time-dependent fashion. Our results indicate that charge coherence must be treated on an equal footing with spin coherence. In particular, we predict the presence of finite-time effects, which result in population transfer even in cases of an incomplete sweep through the anti-crossing. The competing requirements of adiabaticity and coherence are reconciled using specially designed pulses with a tunable level velocity. As a relevant example, we demonstrate that a Hadamard gate can be implemented for a realistic set of conditions in a GaAs double quantum dot device.

I. INTRODUCTION

Electron spins trapped in quantum dots (QDs) are promising candidates for implementing a scalable quantum computer[1,2]. Most of the DiVincenzo criteria have been achieved with spin qubits, including initialization[3], readout[4], and coherent control[5–7]. While experimental progress has been impressive, many of these methods are not yet accurate enough to allow large scale quantum computing with single spins. A key challenge can be appreciated by considering the relevant timescales associated with the spin dynamics. In GaAs quantum dot devices, it is well known that the hyperfine interaction leads to a randomly fluctuating nuclear field, $B_\mathrm{n} \sim 2$ mT, which results in a 10–20 ns spin dephasing time[5,8,9]. For comparison, the Rabi period obtained in a GaAs double quantum dot (DQD) using conventional electron spin resonance (ESR) is on the order of 110 ns[6]. The use of spin-orbit driven electric dipole spin resonance (EDSR) in GaAs leads to even slower Rabi periods of roughly 210 ns[7]. Therefore, in the case of single spin rotations, gate operation times are nearly an order of magnitude slower than the inhomogeneous spin dephasing time. This issue is not specific to GaAs based nanostructures. In InAs nanowires, where the spin-orbit interaction is larger than in GaAs, a Rabi period of $\sim 17\,\mathrm{ns}$ was reported. However, it still is twice as long as the spin dephasing time of $\sim 8\,\mathrm{ns}$[10].

Viewed from a different perspective, the maximum ac field generated in DQD ESR experiments is on the order of 2 mT, which is the same magnitude as the fluctuating nuclear field[6]. As a result, single spin rotations in GaAs qubits follow imperfect trajectories on the Bloch sphere, resulting in a reduced oscillation visibility and gate errors[6]. Single spin selectivity imposes an additional challenge to the development of a spin-based quantum processor. Magnetic fields generated in ESR are difficult to localize on the nanometer scale. Without g-factor control, or local magnetic field gradients, the spins located in a quantum register would rotate at the same rate in the presence of a global ESR field. The long term goal is to be able to drive selective single spin rotations, without affecting neighboring spins that are on average only 20–50 nm away.

Instead of using the spin-up and spin-down states of a single electron, the qubit basis states can be represented by two (out of four) two-electron spin states confined in a double quantum dot (DQD)[11]. For a qubit whose basis states are encoded in the singlet S and triplet T_0 spin states of a DQD, the two-electron exchange interaction allows for a fast 200 ps $\sqrt{\mathrm{SWAP}}$ gate[5]. Recent experiments[12,13] have also demonstrated the possibility of realizing a conditional two-qubit gate. Within this two-spin version of a qubit, the two-qubit gate realized in Ref. 5 can be interpreted as a single qubit operation. However the exchange interaction only allows for rotations about a single axis, whereas to generate arbitrary rotations one needs two perpendicular rotation axes. The generation of a nuclear magnetic field gradient[14] provides rotations about a second, non-collinear axis. While remarkable, this method also presents some difficulties when it has to be extended to a large number of qubits. It requires that the nuclear polarization be controlled in each DQD to create the desired gradient field. An advantage of this method is that the generation of the nuclear field gradient reduces nuclear spin fluctuations, resulting in an increase in the spin dephasing time[15].

Recently, it has been proposed to use a two-spin basis consisting of the singlet S and triplet T_+ spin states[16–18]. Quantum control of the S-T_+ qubit relies on Landau-Zener-Stückelberg-Majorana[19–22] (LZSM) physics, which occurs in the system when the S-T_+ qubit is repeatedly swept through the hyperfine mediated S-T_+ anti-crossing. This method, in addition to being all-electrical, has the advantage of being local.

LZSM physics describing the passage of a two-level quantum system through an anti-crossing can be applied to different fields of physics and chemistry[23]. In quantum information science, LZSM theory accurately describes the observed interference fringes (Stückelberg oscillations) of a superconducting qubit driven back and forth through its anti-crossing[24], as well as the coherent manipulation of a two-spin qubit encoded in the S and triplet T_+ spin states, with dynamics driven by repeated passages through a hyperfine-mediated anti-crossing[16,17].

In this article we develop a master equation to describe partial adiabatic passages between the spin singlet S and triplet T_+ states at the hyperfine mediated anti-crossing in a S-T_+ spin qubit. With our new formalism we show that charge dynamics can significantly hinder LZSM interferometry of spin states. While most of the interesting spin dynamics happens in the $(1,1)$ charge configuration, with one electron per dot, initialization and measurements are done deep in the $(2,0)$ charge configuration, where both electrons are in the left dot. Here (l,r) denotes the number of electrons in the left and right dot. Crossing the $(1,1) \leftrightarrow (2,0)$ interdot charge transition necessarily involves charge dynamics. Since charge states dephase on shorter time scales than spin states, it is essential to consider this fast effective decoherence mechanism while studying spin qubit evolution[25,26]. In particular, we use our formalism to analyze spin-charge dynamics associated with detuning pulses that have a tunable level velocity, with a high level velocity away from the anti-crossing and a slow level velocity in the vicinity of the anti-crossing[18]. Furthermore, we show that this type of pulse is suitable to realize a Hadamard operation, given by the single-qubit unitary

$$H = \frac{1}{\sqrt{2}}\begin{pmatrix} 1 & 1 \\ 1 & -1 \end{pmatrix}, \qquad (1)$$

with a gating time smaller than the characteristic inhomogeneous dephasing time T_2^*. The Hadamard gate is a key element of many quantum algorithms. It is used, for example, in Shor's quantum algorithm for factorizing large integers[27].

The paper is organized as follows. We start by reviewing standard Landau-Zener transition theory, which is valid for an infinitely long ramp through an anti-crossing with a constant level velocity. In Sec. II we review the solution of the finite-time LZSM model, which can be used to model realistic experiments, and we demonstrate within the scope of this theory how fine tuning of the level velocity can be used to increase the visibility of the quantum oscillations. Section III focuses on the physical implementation of LZSM physics in a two-electron spin qubit. We derive an effective Hamiltonian describing the dynamics of the states in the vicinity of the S-T_+ anti-crossing. Compared to previously derived effective Hamiltonians[17], we include the effects of a charge admixture in the spin-dependent anti-crossing. The last part of the section is devoted to the derivation of a master equation that describes the evolution of the density matrix. In Sec. IV we show the results for the singlet return probability obtained from the solution of the master equation and explore the effects of a time-dependent level velocity and charge induced decoherence.

II. ADIABATIC CONTROL OF A QUANTUM TWO-LEVEL SYSTEM

There are numerous problems in physics that deal with the physics of two-level systems. The most common example is Rabi's formula[28] which describes the occupation of a two-level system that is excited by a coherent field. In quantum information science, Rabi oscillations are widely used to manipulate an electron spin confined in a QD[29]. Another widely studied problem involving only two quantum levels is adiabatic passage, which is commonly employed in nuclear magnetic resonance[30]. The physics of adiabatic passage can be found in a variety systems, and several theoretical models have been developed to describe different kinds of adiabatic processes[31–40]. There is however a particular model that has proven to be applicable in many distinct fields of physics, the Landau-Zener[19,20] model. We refer to it in this article as the LZSM model, since it was independently studied by Stückelberg[21] and Majorana[22] in 1932.

The Hamiltonian studied in the LZSM model describes a system with two energy levels [see Fig. 1(a)] that are coupled by an off-diagonal matrix element λ, $H = -\epsilon\sigma_z + \lambda\sigma_x$. Here ϵ is a detuning parameter that is controlled experimentally. The LZSM model considers a detuning sweep described by a constant level velocity, $\alpha = \mathrm{d}(E_2 - E_1)/\mathrm{d}t$, i.e., $\epsilon = \alpha t/2$. The main result of the theory is the asymptotic expression for the non-adiabatic transition probability when the propagation lasts from $t_\mathrm{i} = -\infty$ to $t_\mathrm{f} = \infty$,

$$P_\mathrm{LZSM} = \mathrm{e}^{\frac{-2\pi\lambda^2}{\alpha\hbar}}. \qquad (2)$$

Here we use a generalization of the LZSM model, known as the finite-time LZSM model[41]. It resolves the problem of the energy divergence when $t_\mathrm{f,i} = \pm\infty$, and in contrast to the simple case it gives the relative phase between the states, which is a crucial for predicting the time evolution of any quantum system. Particularly, knowledge of the relative phase is essential in LZSM interferometry[21,23] in which the system is driven back and forth across an anti-crossing. The driving generates quantum interference between states which are directly observable in the non-adiabatic (or adiabatic) transition probability.

A. Finite-time Landau-Zener-Stückelberg-Majorana propagator

The unitary evolution operator defined by the LZSM Hamiltonian[19–22],

$$H(t) = \begin{pmatrix} -\frac{\alpha}{2}t & \lambda \\ \lambda & \frac{\alpha}{2}t \end{pmatrix}, \qquad (3)$$

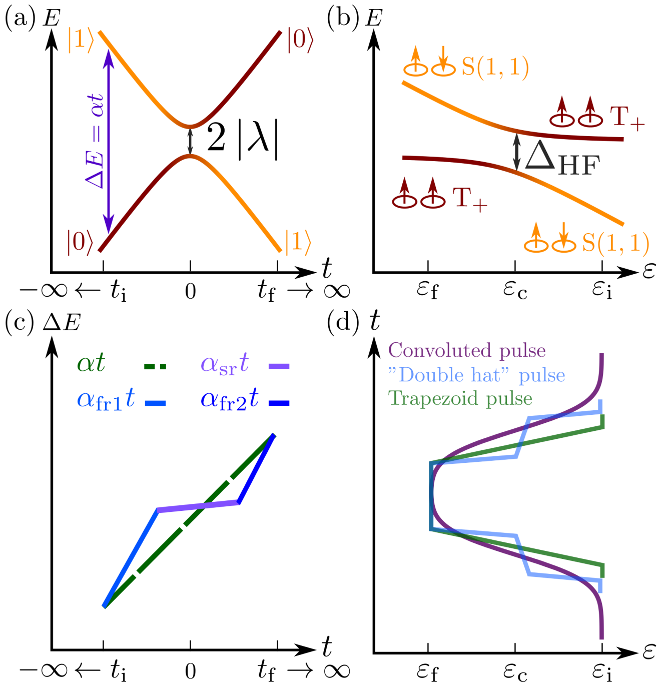

Figure 1. (color online) (a) The Landau-Zener-Stückelberg-Majorana (LZSM) problem. The LZSM model addresses the problem of a two-level system that is swept through an anti-crossing. It assumes an infinitely long ramp (i.e. propagation from $t_{\mathrm{i}} \rightarrow -\infty$ to $t_{\mathrm{f}} \rightarrow \infty$), a constant coupling constant λ leading to a splitting $2\,|\lambda|$ at $t = 0$, and an energy difference between the levels which is linear in time $\Delta E(t) = \alpha t$. Its main result yields the non-adiabatic transition probability, P_{LZSM}. An extension of the model to finite-times resolves the problem of infinite energies and undefined phases. (b) Singlet and triplet T_+ energies in a DQD as a function of detuning ε, where $\varepsilon_{\mathrm{i}} = \varepsilon(t_{\mathrm{i}})$ and $\varepsilon_{\mathrm{f}} = \varepsilon(t_{\mathrm{f}})$. The two-electron DQD is a physical realization of the LZSM model. Here, the hyperfine coupling of the two spin states leads to a splitting Δ_{HF}. (c) The LZSM model assumes a constant level velocity α. In order to increase adiabaticity one can lower alpha, but in order to keep short pulses it is preferable to use multi rise-time pulses. (d) Comparison of possible pulses that can be used to manipulate the singlet triplet T_+ qubit. In terms of total propagation time, "double hat" pulses represent a good compromise between conventional trapezoid and convoluted pulses.

is given by[41]

$$U(t_{\mathrm{f}},\, t_{\mathrm{i}}) = \begin{pmatrix} u_{11}(t_{\mathrm{f}},\, t_{\mathrm{i}}) & u_{12}(t_{\mathrm{f}},\, t_{\mathrm{i}}) \\ u_{21}(t_{\mathrm{f}},\, t_{\mathrm{i}}) & u_{22}(t_{\mathrm{f}},\, t_{\mathrm{i}}) \end{pmatrix}, \tag{4}$$

with

$$\begin{aligned} &u_{11}(t_{\mathrm{f}},\, t_{\mathrm{i}}) = u_{22}^{*}(t_{\mathrm{f}},\, t_{\mathrm{i}}) = \\ &\frac{\Gamma\left(1 - \mathrm{i}\eta^2\right)}{\sqrt{2\pi}} \Big[D_{\mathrm{i}\eta^2}\left(\mathrm{e}^{\frac{-\mathrm{i}\pi}{4}} \tau_{\mathrm{f}}\right) D_{\mathrm{i}\eta^2 - 1}\left(\mathrm{e}^{\frac{3\mathrm{i}\pi}{4}} \tau_{\mathrm{i}}\right) \\ &+ D_{\mathrm{i}\eta^2}\left(\mathrm{e}^{\frac{3\mathrm{i}\pi}{4}} \tau_{\mathrm{f}}\right) D_{\mathrm{i}\eta^2 - 1}\left(\mathrm{e}^{-\frac{\mathrm{i}\pi}{4}} \tau_{\mathrm{i}}\right) \Big] \end{aligned} \tag{5}$$

and

$$\begin{aligned} &u_{12}(t_{\mathrm{f}},\, t_{\mathrm{i}}) = -u_{21}^{*}(t_{\mathrm{f}},\, t_{\mathrm{i}}) = \\ &\frac{\Gamma\left(1 - \mathrm{i}\eta^2\right)}{\sqrt{2\pi}\eta} \mathrm{e}^{\frac{\mathrm{i}\pi}{4}} \Big[-D_{\mathrm{i}\eta^2}\left(\mathrm{e}^{\frac{-\mathrm{i}\pi}{4}} \tau_{\mathrm{f}}\right) D_{\mathrm{i}\eta^2}\left(\mathrm{e}^{\frac{3\mathrm{i}\pi}{4}} \tau_{\mathrm{i}}\right) \\ &+ D_{\mathrm{i}\eta^2}\left(\mathrm{e}^{\frac{3\mathrm{i}\pi}{4}} \tau_{\mathrm{f}}\right) D_{\mathrm{i}\eta^2}\left(\mathrm{e}^{-\frac{\mathrm{i}\pi}{4}} \tau_{\mathrm{i}}\right) \Big]. \end{aligned} \tag{6}$$

Here $\tau = \sqrt{\alpha/\hbar} t$ is a dimensionless time, $\eta = \lambda/\sqrt{\alpha\hbar}$ is a dimensionless coupling, $\Gamma(z)$ is the gamma function[42], and $D_{\nu}(z)$ is the parabolic cylinder function[43].

The LZSM propagator fully determines the partially adiabatic dynamics of a quantum two-level system. In the case where the two-level system encodes a qubit, Eq. (4) allows the design of single qubit operations. This method has been used to control superconducting qubits[23,24], and more recently to implement a qubit encoded in the spin of a two-electron state[16,17]. However, since the spin states are weakly coupled, $\eta < 1$, it is hard to achieve an equally weighted coherent superposition of spin states and fully explore the entire qubit state space. In order to achieve full control over the spin qubit, it would be necessary to increase η by making α smaller. However, the LZSM equation requires an exponential increase in the propagation time in order to achieve a fully adiabatic transition. In a real physical system, this method is unpractical because the pulse duration should remain shorter than the coherence time of the two-level system.

B. Enhancing Adiabatic Control

As demonstrated in Ref. 18, it is possible to use more complex pulses to increase the balance of the populations while keeping the manipulation time below the decoherence times. The key idea relies on an observation based on the finite-time LZSM model. For a slow level velocity α, which favors adiabatic passage, most of the population change occurs in the vicinity of the anti-crossing. It is therefore possible to use detuning pulses that have a time-dependent level velocity. Let us consider two types of pulses, as illustrated in Fig 1(c) and (d)). The first is a conventional linear pulse, which is standard in LZSM theory. The second pulse profile consists of linear detuning ramps in a fast-slow-fast rise-time sequence, which we refer to as multi-ramp pulse. The unitary evolution of such a general sequence can be written using Eq. (4) as

$$\begin{aligned} U(t_{\mathrm{f}}, t_{\mathrm{i}}) &= U_{\mathrm{fast2}}(t_{\mathrm{f}},\, t_2) U_{\mathrm{slow}}(t_2,\, t_1) U_{\mathrm{fast1}}(t_1,\, t_{\mathrm{i}}) \\ &= \begin{pmatrix} \tilde{u}_{11}(t_{\mathrm{f}},\, t_{\mathrm{i}}) & \tilde{u}_{12}(t_{\mathrm{f}},\, t_{\mathrm{i}}) \\ \tilde{u}_{21}(t_{\mathrm{f}},\, t_{\mathrm{i}}) & \tilde{u}_{22}(t_{\mathrm{f}},\, t_{\mathrm{i}}) \end{pmatrix}. \end{aligned} \tag{7}$$

Here $t_1 = t_{\mathrm{fr1}}$, $t_2 = t_{\mathrm{fr1}} + t_{\mathrm{sr}}$, and $t_{\mathrm{f}} = t_{\mathrm{fr1}} + t_{\mathrm{sr}} + t_{\mathrm{fr2}}$, where $t_{\mathrm{fr}j}$ is the propagation time associated to the jth fast sequence, and t_{sr} corresponds to the slow sequence. We use this notation to refer to the corresponding level

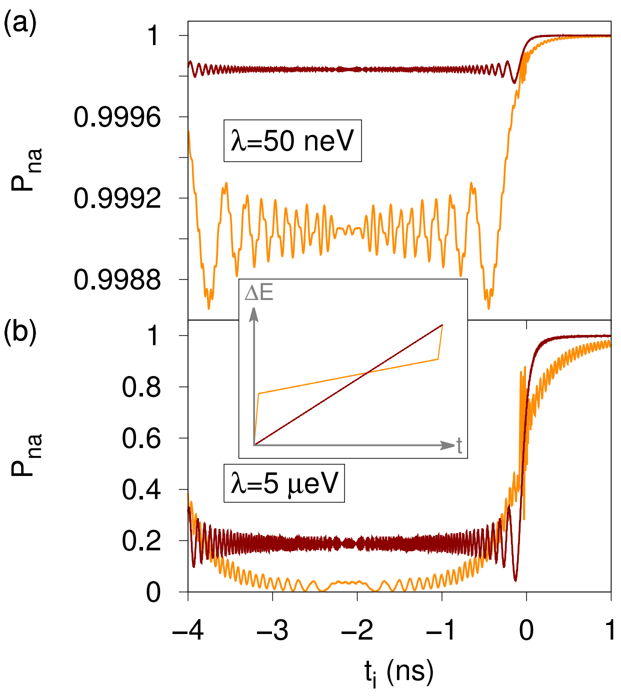

Figure 2. (color online) (a) Comparison of the non-adiabatic transition probability, P_{na}, for a "double ramp" (orange) and a linear pulse (red) as function of t_{i}. Here, $t_1 - t_{\mathrm{i}} = 0.1\,\mathrm{ns}$, $t_2 - t_1 = 2.0\,\mathrm{ns}$, $t_{\mathrm{f}} - t_2 = 0.1\,\mathrm{ns}$, $\lambda = 50\,\mathrm{neV}$, $\alpha_{\mathrm{fr1}} = 3 \cdot 10^6\,\mathrm{eVs}^{-1}$, $\alpha_{\mathrm{sr}} = 5 \cdot 10^4\,\mathrm{eVs}^{-1}$, and $\alpha_{\mathrm{fr2}} = 2 \cdot 10^6\,\mathrm{eVs}^{-1}$. The condition that the system must reach the same difference in energy defines the level velocity for the Gaussian pulse. The double hat pulse sequence increases the adiabatic transition probability, while keeping the total propagation time fixed. (b) In the strong coupling regime the double hat pulse allows full adiabatic population transfer by fine tuning t_{i}. Here $\lambda = 5\,\mu\mathrm{eV}$ and $t_2 - t_1 = 4.0\,\mathrm{ns}$, the others parameters are the same as in (a). (inset) Schematic representation of the pulses used to obtain non-adiabatic probabilities. The colors of the pulses are matched to the results shown in (a) and (b).

velocities α_j, dimensionless times τ_j, and dimensionless couplings η_j.

To illustrate the advantage of a multi-ramp pulse, we plot in Fig. 2 the non-adiabatic transition probability, $P_{\mathrm{na}} = |u_{11}(t_{\mathrm{i}}, t_{\mathrm{f}})|^2$, as a function of t_{i} for two different coupling constants. Here a non-adiabatic transition refers to a transition where the system remains in the initial uncoupled energy eigenstate. The level velocity for the linear pulse, α_{si} is obtained by the condition that the system must be detuned to the same difference in energy,

$$\alpha_{\mathrm{si}} = \frac{\alpha_{\mathrm{fr1}} t_{\mathrm{fr1}} + \alpha_{\mathrm{sr}} t_{\mathrm{sr}} + \alpha_{\mathrm{fr2}} t_{\mathrm{fr2}}}{t_{\mathrm{f}} - t_{\mathrm{i}}}. \tag{8}$$

We start considering a weak coupling regime for the slow component of the pulse, $\eta_{\mathrm{sr}} < 1$. The results are presented in Fig. 2(a), where we have chosen $t_1 - t_{\mathrm{i}} = 0.1\,\mathrm{ns}$, $t_2 - t_1 = 2.0\,\mathrm{ns}$, $t_{\mathrm{f}} - t_2 = 0.1\,\mathrm{ns}$, $\lambda = 50\,\mathrm{neV}$, $\alpha_{\mathrm{fr1}} = 3 \cdot 10^6\,\mathrm{eVs}^{-1}$, $\alpha_{\mathrm{sr}} = 5 \cdot 10^4\,\mathrm{eVs}^{-1}$, and $\alpha_{\mathrm{fr2}} = 2 \cdot 10^6\,\mathrm{eVs}^{-1}$. Although the passage through the anti-crossing is done under conditions that largely favor non-adiabatic transition, the multi-ramp pulse leads to a more adiabatic passage than a linear pulse with the same total propagation time $\Delta t = t_{\mathrm{f}} - t_{\mathrm{i}}$.

All the interest of the method lies on this last property, if we think of a two-level quantum system as a physical implementation of a qubit. Since a qubit cannot be perfectly isolated from its environment, any coherent state is going to decohere within a characteristic time scale. In the case of LZSM driven qubits, this implies that there must be a compromise between the optimal time to realize a quantum operation and the decoherence time. However, the use of multi-ramp pulses allows an increase in adiabaticity while keeping propagation times smaller than decoherence times.

This control method is more efficient in the case of strong coupling, $\eta_{\mathrm{sr}} > 1$. It allows to achieve fast full population transfer by fine tuning of t_{i} (or t_{f}). We present in Fig. 2(b) results obtained for P_{na} as a function of t_{i} for $\lambda = 5\,\mu\mathrm{eV}$ and $t_2 - t_1 = 4.0\,\mathrm{ns}$. A method allowing for high fidelity full population transfer using composite chirped pulses has also been proposed[44].

III. ADIABATIC CONTROL OF A $\mathrm{S} - \mathrm{T}_+$ QUBIT

In the following, we apply the previously developed ideas to a physical implementation of a LZSM driven qubit. We focus on the two-spin $\mathrm{S} - \mathrm{T}_+$ implementation in a GaAs DQD[16,17], see Fig. 1(b). Although the dynamics of the system under multi rise-time pulses has already been studied experimentally[18], there is still a need to gain a better understanding of the charge-noise-induced spin dephasing. We will show, among other things, that the measurement of finite-time LZSM oscillations can provide a tool to qualitatively define the strength of charge noise.

A. Double Quantum Dot Spin States

The spin preserving part of the Hamiltonian describing the confinement of electrons in a DQD in the presence of an external magnetic field can be written using a simple two-site hopping model,

$$\begin{aligned} H_0 = &\sum_{\substack{i=1,2 \\ \sigma=\uparrow,\downarrow}} \left(\varepsilon_i + \frac{1}{2} g^* \mu_{\mathrm{B}} B \sigma\right) c^\dagger_{i\sigma} c_{i\sigma} + u \sum_i c^\dagger_{i\uparrow} c_{i\uparrow} c^\dagger_{i\downarrow} c_{i\downarrow} \\ &+ \tau \sum_\sigma \left(c^\dagger_{1\sigma} c_{2\sigma} + \mathrm{h.c.}\right). \end{aligned} \tag{9}$$

The index $i = 1, 2$ labels the dot number and $\sigma = \uparrow, \downarrow = \pm 1$ the spin of the electron. We denote the energy of a single confined electron by ε_i and the Zeeman energy associated with its spin is given by $g^* \mu_{\mathrm{B}} B \sigma / 2$, where g^*

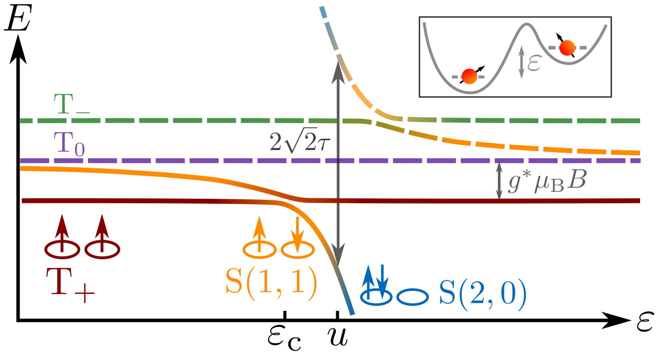

Figure 3. (color online) (a) Energy diagram for the relevant states in the DQD as a function of ε. The spin states for the implementation of the qubit are the hybridized singlet S and the triplet T_+.

denotes the effective Landé g-factor, μ_B the Bohr magneton, B the strength of the external magnetic field. The operators $c_{i\sigma}$ and $c_{i\sigma}^\dagger$ describe respectively the annihilation and creation of an electron in dot i with spin σ. Two electrons occupying the same QD cost an intra-dot Coulomb energy u. The last term of Eq. (9) accounts for electron tunneling between the dots with strength τ. We neglect the inter-dot Coulomb interaction because it only produces a constant shift of the energy levels.

Since most recent experiments on a DQD system are operated in a regime with at most two electrons, we can project Eq. (9) into the subspace spanned by the charge configurations $(0,2)$, $(2,0)$, and $(1,1)$[5,14,16,45,46]. The diagonalization of the resulting Hamiltonian leads to six low-energy states which are superpositions of the singlets $\mathrm{S}(0,2)$, $\mathrm{S}(2,0)$, and $\mathrm{S}(1,1)$ as well as the triplets $\mathrm{T}_0(1,1)$, $\mathrm{T}_+(1,1)$, and $\mathrm{T}_-(1,1)$. The triplet states with two particles in the same dot must have electrons occupying higher-energy orbitals levels due to the Pauli principle. This results in a relatively high separation in energy ($\sim 400\,\mu$eV) from a singlet with both electrons occupying the same dot[47]. Consequently the triplets states with two electrons in the same dot can be safely neglected for the purpose of the current study.

An energy level diagram is shown in Fig. 3, where we plot the energies of the relevant two-electron spin states as a function of detuning $\varepsilon = \varepsilon_1 - \varepsilon_2$. The degeneracy of the singlets $\mathrm{S}(1,1)$ and $\mathrm{S}(2,0)$ at $\varepsilon = u$, as well as between $\mathrm{S}(1,1)$ and $\mathrm{S}(0,2)$ at $\varepsilon = -u$, is lifted due to tunneling, which results in a splitting of the levels by $2\sqrt{2}\tau$. The degeneracy between the spin singlet S and spin triplet T_0 is lifted due to the exchange interaction[48]. This property has allowed the encoding of a spin qubit in these two spin states and its manipulation it via the exchange interaction[5].

Here we concentrate on a particular value of detuning that we have denoted by ε_c in the energy level diagram. This point corresponds to the crossing of the singlet state with the triplet T_+ state. What renders this point special is that in reality there is an anti-crossing due to the hyperfine interaction between the electron spins and nuclear spins of the host material. It has been demonstrated experimentally[16] and theoretically[17] that coherent control of the singlet S and triplet T_+ can be achieved by detuning the system from an initially prepared $\mathrm{S}(2,0)$ through the hyperfine mediated anti-crossing.

The hyperfine interaction is described by the Hamiltonian

$$H_\mathrm{HF} = \boldsymbol{S}_1 \cdot \boldsymbol{h}_1 + \boldsymbol{S}_2 \cdot \boldsymbol{h}_2 \tag{10}$$

between the electron spin $\boldsymbol{S}_i$ and the effective magnetic fields $\boldsymbol{h}_i$ that are generated by the nuclear spins $\boldsymbol{I}_i$ in dot i. The Overhauser field operators $\boldsymbol{h}_i = \sum_{k=1}^{n_i} A_i^k \boldsymbol{I}_i^k$ describe the nuclear bath. Here n_i is the number of nuclei in dot i and $A_i^k = v_{ik}\nu_0 \left|\psi_i(\boldsymbol{r}_k)\right|^2$ is the hyperfine coupling constant with the k-th nucleus in dot i, with $\psi_i(\boldsymbol{r}_k)$ the electron wave function, ν_0 the volume of the unit cell and v_{ik} the hyperfine coupling strength. A more convenient form of the hyperfine interaction is obtained by introducing the spin ladder operators $S_i^\pm = S_i^x \pm \mathrm{i}S_i^y$ and $h_i^\pm = h_i^x \pm \mathrm{i}h_i^y$, which yields

$$H_\mathrm{HF} = \frac{1}{2}\sum_i \left(2S_i^z h_i^z + S_i^+ h_i^- + S_i^- h_i^+\right). \tag{11}$$

The longitudinal part of H_HF is diagonal and its contribution will add to the energy of the triplet state. The transverse part

$$H_\mathrm{HF}^\perp = \sum_i (S_i^+ h_i^- + S_i^- h_i^+), \tag{12}$$

generates the so-called flip-flop process that result in an energy gap at ε_c and allow for mixing of the S and T_+ spin states[8,9,15].

B. $\mathrm{S} - \mathrm{T}_+$ Effective Hamiltonian

In order to derive the Hamiltonian describing the dynamics of the two-electron spin states near the hyperfine induced anti-crossing, we consider a 3×3 Hamiltonian

$$H_0(\varepsilon) \simeq \begin{pmatrix} g^*\mu_\mathrm{B}B & 0 & 0 \\ 0 & 0 & \sqrt{2}\tau \\ 0 & \sqrt{2}\tau & u-\varepsilon \end{pmatrix} \tag{13}$$

which accounts for the dynamics of the $\mathrm{T}_+(1,1)$, $\mathrm{S}(1,1)$, and $\mathrm{S}(2,0)$ spin states in an external magnetic field, B.

The diagonalization of Eq. (13) yields two hybridized singlets and the triplet state T_+

$$|\mathrm{S}\rangle = c(\varepsilon)|\mathrm{S}(1,1)\rangle + \sqrt{1-c(\varepsilon)^2}|\mathrm{S}(2,0)\rangle, \tag{14}$$

$$|\mathrm{S}'\rangle = c'(\varepsilon)|\mathrm{S}(1,1)\rangle + \sqrt{1-c'(\varepsilon)^2}|\mathrm{S}(2,0)\rangle, \tag{15}$$

$$|\mathrm{T}\rangle = |\mathrm{T}_+(1,1)\rangle, \tag{16}$$

with respective energies

$$E_{\mathrm{S}}(\varepsilon) = \frac{1}{2}(u - \varepsilon - \sqrt{8\tau^2 + (u-\varepsilon)^2}), \tag{17}$$

$$E_{\mathrm{S}'}(\varepsilon) = \frac{1}{2}(u - \varepsilon + \sqrt{8\tau^2 + (u-\varepsilon)^2}), \tag{18}$$

$$E_{\mathrm{T}} = g^* \mu_{\mathrm{B}} B. \tag{19}$$

The charge admixture coefficients $c(\varepsilon)$ and $c'(\varepsilon)$ are

$$c(\varepsilon) = \frac{\varepsilon - u - \sqrt{8\tau^2 + (u-\varepsilon)^2}}{\sqrt{8\tau^2 + (-\varepsilon + u + \sqrt{8\tau^2 + (\varepsilon - u)^2})^2}}, \tag{20}$$

$$c'(\varepsilon) = \frac{\varepsilon - u + \sqrt{8\tau^2 + (u-\varepsilon)^2}}{\sqrt{8\tau^2 + (\varepsilon + u + \sqrt{8\tau^2 + (\varepsilon - u)^2})^2}}. \tag{21}$$

We can now make the following basis change

$$T(\varepsilon) = \begin{pmatrix} 1 & 0 & 0 \\ 0 & c(\varepsilon) & c'(\varepsilon) \\ 0 & \sqrt{1 - c^2(\varepsilon)} & \sqrt{1 - c'^2(\varepsilon)} \end{pmatrix}, \tag{22}$$

such that

$$\begin{aligned} H_0^{\mathrm{diag}}(\varepsilon) &= T(\varepsilon)^\dagger H_0(\varepsilon) T(\varepsilon) \\ &= \begin{pmatrix} g^*\mu_{\mathrm{B}} B & 0 & 0 \\ 0 & E_{\mathrm{S}} & 0 \\ 0 & 0 & E_{\mathrm{S}'} \end{pmatrix}. \end{aligned} \tag{23}$$

We add now to the Hamiltonian defined in Eq. (13) the hyperfine interaction defined in Eq. (10). Since we are not interested in describing the nuclear spins dynamics, but its effect on the two-spin states S and T_+, we can model the action of the Overhauser field operators by introducing a classical stochastic variable which accounts for fluctuations in the nuclear spin ensemble[8,9,15]. By setting

$$\boldsymbol{h}_i = g^* \mu_{\mathrm{B}} \mathbf{B}_{\mathrm{n},i}, \tag{24}$$

we can interpret $\mathbf{B}_{\mathrm{n},i}$ as the effective random magnetic field interacting on $\boldsymbol{S}_i$. Under normal experimental conditions we have $k_{\mathrm{B}}T \gg g_{\mathrm{n}}\mu_{\mathrm{n}}B$, where g_{n} and μ_{n} are the nuclear g-factor and magneton. The nuclei can, in this limit, be assumed to be completely unpolarized, resulting in a Gaussian distribution of nuclear fields[8,9,15]

$$p(B_{\mathrm{n},\,i}) = \frac{1}{\sqrt{2\pi}\sigma} \mathrm{e}^{-\frac{B_{\mathrm{n},\,i}^2}{2\sigma^2}}, \tag{25}$$

with $\sigma = A/g^*\mu_{\mathrm{B}}\sqrt{n}$ and the hyperfine coupling constant $A \approx 90\,\mu$eV, and the approximate number of nuclei overlapping with the electronic wave function $n \approx 10^5 - 10^6$. By defining $B^{\pm}_{\mathrm{n},\,i} = B^x_{\mathrm{n},\,i} \pm \mathrm{i} B^y_{\mathrm{n},\,i}$, the hyperfine Hamiltonian can be written by analogy with Eq. (11) as

$$H_{\mathrm{HF}} = \frac{1}{2}\sum_i \left(2S_i^z B^z_{\mathrm{n},i} + S_i^+ B^-_{\mathrm{n},i} + S_i^- B^+_{\mathrm{n},i}\right). \tag{26}$$

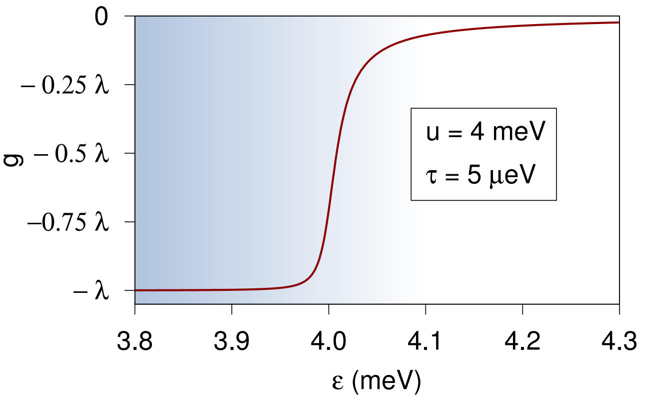

Figure 4. (color online) The effective hyperfine mediated coupling between |S⟩ and |T⟩ is a function of detuning. This is a consequence of the state |S⟩ being an superposition of different charge states.

The longitudinal part of H_{HF} can be included in the energy of the triplet state $g^*\mu_{\mathrm{B}}B \rightarrow g^*\mu_{\mathrm{B}}(B + B^z_{\mathrm{n},1} + B^z_{\mathrm{n},2})$, while the transverse part

$$H^{\perp}_{\mathrm{HF}} = \sum_i (S_i^+ B^-_{\mathrm{n},i} + S_i^- B^+_{\mathrm{n},i}). \tag{27}$$

mixes the spin states |S⟩ and |T⟩. We therefore find that the full Hamiltonian, in the $\{\mathrm{T}_+(1,1), \mathrm{S}(1,1), \mathrm{S}(2,0)\}$ basis, describing the dynamics of the singlet S and triplet T_+ near the hyperfine anti-crossing is given by

$$H_{\mathrm{S-T_+}}(\varepsilon) = \begin{pmatrix} g^*\mu_{\mathrm{B}}\tilde{B} & \lambda & 0 \\ \lambda & 0 & \sqrt{2}\tau \\ 0 & \sqrt{2}\tau & (u - \varepsilon) \end{pmatrix}, \tag{28}$$

where $\tilde{B} = B + B^z_{\mathrm{n},1} + B^z_{\mathrm{n},2}$ and

$$\lambda = \langle \mathrm{S}(1,1)|H^{\perp}_{\mathrm{HF}}|\mathrm{T}_+(1,1)\rangle = g^*\mu_{\mathrm{B}}(B^-_{\mathrm{n},2} - B^-_{\mathrm{n},1})/2\sqrt{2}. \tag{29}$$

In the basis that diagonalizes Eq. (13), the Hamiltonian defined in Eq. (28) reads

$$\tilde{H}_{\mathrm{S-T_+}}(\varepsilon) = \begin{pmatrix} g^*\mu_{\mathrm{B}}\tilde{B} & c(\varepsilon)\lambda & d(\varepsilon)\lambda \\ c(\varepsilon)\lambda & E_{\mathrm{S}}(\varepsilon) & 0 \\ d(\varepsilon)\lambda & 0 & E_{\mathrm{S}'}(\varepsilon) \end{pmatrix}. \tag{30}$$

The projection of Eq. (30) onto the Hilbert space spanned by {|S⟩, |T⟩} leads to the effective 2 × 2 Hamiltonian describing the dynamics at the singlet-triplet T_+ anti-crossing. The higher energy singlet state |S′⟩ can be safely neglected if the pulses bringing the states |S⟩ and |T⟩ into resonance are fully adiabatic with respect to the energy separation $\Delta E_{\mathrm{SS}'} = 2\sqrt{2}\tau$ of |S⟩ and |S′⟩ at the charge anti-crossing. Taking into account that the detuning is time-dependent, $\varepsilon = \varepsilon(t)$, we finally obtain

$$H(t) = E_{\mathrm{S}}(\varepsilon(t))|\mathrm{S}\rangle\langle\mathrm{S}| + \tilde{E}_{\mathrm{T}}|\mathrm{T}\rangle\langle\mathrm{T}| + g(\varepsilon(t))\left(|\mathrm{S}\rangle\langle\mathrm{T}| + \mathrm{h.c}\right), \tag{31}$$

where E_{S} is defined in Eq. (17) and $\tilde{E}_{\mathrm{T}} = g^* \mu_{\mathrm{B}} \tilde{B}$. This effective Hamiltonian differs form previous derivations[17,49] in the coupling $g(t) = c(\varepsilon(t))\lambda$, which is time-dependent. Here, $c(\varepsilon(t))$ and λ are given in Eqs. (20) and (29). As it can be seen from the functional form of $g(t)$, the effective coupling strength between the spin states depends on the charge state (Fig. 4). This result is rather natural since the matrix element between S and T_+ goes to zero when the detuning is such that $\mathrm{S} = \mathrm{S}(2,0)$ and $\mathrm{T}_+ = \mathrm{T}_+(1,1)$, i.e., $\langle \mathrm{S}|H_{\mathrm{HF}}^{\perp}|\mathrm{T}_+\rangle \to 0$ for $\varepsilon \gg u$. It also implies that the physics described by Eq. (31) goes beyond standard LZSM theory with a constant coupling. However, since both Hamiltonians describe adiabatic passage through an anti-crossing, we can assume that the dynamics are qualitatively similar. We can therefore expect that our previous discussion about enhancement of adiabaticity based on LZSM physics remains valid. Furthermore, due to the peculiar form of $g(t)$ (c.f. Fig. 4), we can assume that it is possible to observe finite-time interferometry phenomena in close vicinity of the anti-crossing.

C. Master Equation

In order to compare our theory with experimental measurements, it is not sufficient to solve the Hamiltonian dynamics provided by Eq. (31), because some important phenomena that can influence the outcome of the experiment are not taken into account. Among these is the spin-orbit interaction that leads to phonon mediated relaxation and charge fluctuations that lead to dephasing of a charge superposition state. These phenomena can be taken into account in a master equation formalism for the density matrix. In the Lindblad formalism, the time evolution can be expressed as

$$\dot{\rho} = -\frac{\mathrm{i}}{\hbar}\left[H,\rho\right] + \frac{1}{2}\sum_{j=1}^{N^2-1}\left(\left[L_j\rho, L_j^\dagger\right] + \left[L_j, \rho L_j^\dagger\right]\right). \tag{32}$$

The operators L_j are called Lindblad operators[50,51] and they describe the dissipative effect of the environment on the system in the Born-Markov approximation, which consists of two assumptions that lead to Eq. (32). The Born approximation supposes a weak coupling between the system and the bath, in the case of spin-orbit interaction to the phonon bath, while the Markov approximation consists in neglecting any type of memory effects of the bath during the system evolution. To fully describe the effect of the environment, one needs $N^2 - 1$ operators where N is the dimension of the system's Hilbert space[50,51]. For the case of a two-level system, the Lindblad operators are $L_1 = \sqrt{\Gamma_-}\sigma_-$, $L_2 = \sqrt{\Gamma_+}\sigma_+$, and $L_3 = \sqrt{\Gamma_\varphi}\sigma_z$, where σ_- and σ_+ are spin ladder operators and σ_z is the z Pauli matrix. They respectively describe relaxation from the excited state to the ground state with rate Γ_-, relaxation from the ground state to the excited state with rate Γ_+, and pure dephasing with rate Γ_φ.

By substituting Eq. (31) into Eq. (32) and using the expression of the Lindblad operators, the first order differential equation for the S-T_+ density matrix can be written as

$$\begin{pmatrix}\dot{\rho}_{11}\\ \dot{\rho}_{12}\\ \dot{\rho}_{21}\\ \dot{\rho}_{22}\end{pmatrix} = \begin{pmatrix} -\Gamma_+ & \frac{\mathrm{i}}{\hbar}g(t) & -\frac{\mathrm{i}}{\hbar}g(t) & \Gamma_- \\ \frac{\mathrm{i}}{\hbar}g(t) & -\frac{\mathrm{i}}{\hbar}(E_{\mathrm{S}}(t)-\tilde{E}_{\mathrm{T}}) - \frac{1}{2}\left(\Gamma_+ + \Gamma_- + 4\Gamma_\varphi\right) & 0 & -\frac{\mathrm{i}}{\hbar}g(t) \\ -\frac{\mathrm{i}}{\hbar}g(t) & 0 & \frac{\mathrm{i}}{\hbar}(E_{\mathrm{S}}(t)-\tilde{E}_{\mathrm{T}}) - \frac{1}{2}\left(\Gamma_+ + \Gamma_- + 4\Gamma_\varphi\right) & \frac{\mathrm{i}}{\hbar}g(t) \\ \Gamma_+ & -\frac{\mathrm{i}}{\hbar}g(t) & \frac{\mathrm{i}}{\hbar}g(t) & -\Gamma_- \end{pmatrix}\begin{pmatrix}\rho_{11}\\ \rho_{12}\\ \rho_{21}\\ \rho_{22}\end{pmatrix}, \tag{33}$$

where we denote the uncoupled ground state and excited states with the indices 1 and 2. This system of four coupled ordinary differential equations can be reduced to a system of three coupled ordinary differential equations (Bloch equations) by introducing new variables defined by

$$\begin{aligned} x &= \rho_{12} + \rho_{21}, \\ y &= \mathrm{i}\left(\rho_{12} - \rho_{21}\right), \\ z &= \rho_{11} - \rho_{22}. \end{aligned} \tag{34}$$

This set of variables is completed by the conservation of probability condition,

$$\rho_{11} + \rho_{22} = 1. \tag{35}$$

Substituting Eqs. (34) and (35) into Eq. (33), one finds the system of ordinary differential equations for the new variables,

$$\dot{x} = -\frac{E_{\mathrm{S}} - \tilde{E}_{\mathrm{T}}}{\hbar}y - \frac{1}{2}\left(\Gamma_+ + \Gamma_-\right)x - 2\Gamma_\varphi x, \tag{36}$$

$$\dot{y} = \frac{E_{\mathrm{S}} - \tilde{E}_{\mathrm{T}}}{\hbar}x - 2\frac{g}{\hbar}z - \frac{1}{2}\left(\Gamma_+ + \Gamma_-\right)y - 2\Gamma_\varphi y, \tag{37}$$

$$\dot{z} = 2\frac{g}{\hbar}y - \left(\Gamma_+ + \Gamma_-\right)z + \Gamma_- - \Gamma_+. \tag{38}$$

Since Γ_+ and Γ_- can be related to each other by considering the limiting case of thermal equilibrium, Eqs. (36)–(38) can be simplified to include only two independent rates. If the system reaches thermal equilibrium then the detailed balance equation $\rho_{11}^{\mathrm{th}}\Gamma_+ = \rho_{22}^{\mathrm{th}}\Gamma_-$ holds. Moreover, the populations are given by the canonical ensem-

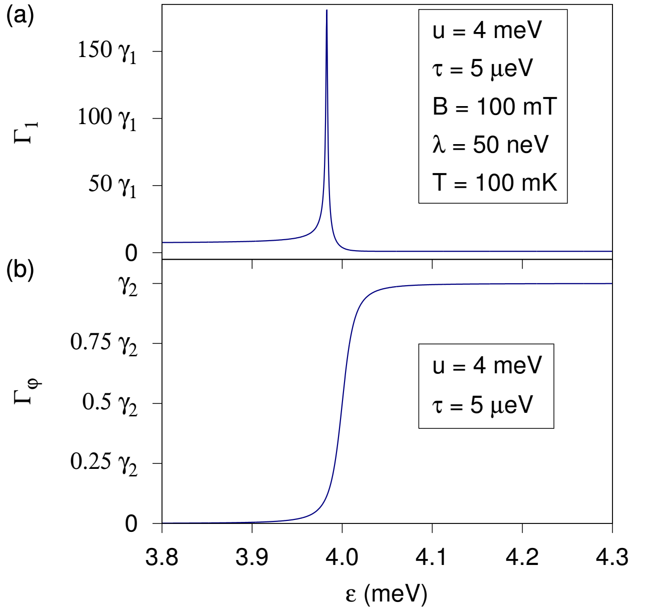

Figure 5. (color online) (a) Relaxation rate $\Gamma_1(\varepsilon)$ obtained for $B = 100\,\mathrm{mT}$. Spin-orbit mediated flip-flops of the electron spin accompanied by emission or absorption of phonons is assumed to be the leading relaxation mechanism. The relaxation rate is maximal for $\varepsilon = \varepsilon_{\mathrm{c}}$ where $\left|E_{\mathrm{S}}^{d}(\varepsilon) - E_{\mathrm{T}}^{d}\right| \ll k_{\mathrm{B}}T$. This results in a strong mixing of the spin states due to thermal fluctuations. (b) Charge noise induced dephasing rate $\Gamma_2(\varepsilon)$. The dephasing rate is assumed to have a functional dependence proportional to $1 - c(\varepsilon)^2$ to ensure that dephasing related to a charge noise is suppressed when the system is in a $(1,1)$ charge configuration.

ble, $\rho_{ii}^{\mathrm{th}} = \exp(-\beta E_i)/Z$, where $\beta = 1/k_{\mathrm{B}}T$, where k_{B} is Boltzman's constant, T is the temperature, and Z is the partition function. This yields

$$\frac{\Gamma_+}{\Gamma_-} = \frac{\rho_{22}^{\mathrm{th}}}{\rho_{11}^{\mathrm{th}}} = \mathrm{e}^{-\beta\hbar\omega}, \tag{39}$$

where we used $\hbar\omega = \left|E_{\mathrm{S}}^{d} - E_{\mathrm{T}}^{d}\right|$. The energies E_{S}^{d} and E_{T}^{d} are obtained by diagonalizing Eq. (31).

Since Γ_- is associated with a process involving the emission of a phonon, we can express it as

$$\Gamma_- = \gamma_1\left(1 + n(\omega)\right), \tag{40}$$

where $n(\omega)$ is the Bose-Einstein occupation number, $n(\omega) = (\exp(\beta\hbar\omega) - 1)^{-1}$, and γ_1 is the spontaneous decay rate, which we treat as a phenomenological parameter here. Similarly we obtain

$$\Gamma_+ = \gamma_1 n(\omega). \tag{41}$$

Combining the results of Eqs. (39), (40), and (41), we obtain the relaxation rate

$$\Gamma_1(\varepsilon) = \Gamma_+ + \Gamma_- = \gamma_1 \coth\left(\frac{\left|E_{\mathrm{S}}^{d}(\varepsilon) - E_{\mathrm{T}}^{d}(\varepsilon)\right|}{2k_{\mathrm{B}}T}\right). \tag{42}$$

This function is plotted against ε in Fig. 5a, and has a peak at $\varepsilon = \varepsilon_{\mathrm{c}}$ where $\left|E_{\mathrm{S}}^{d}(\varepsilon) - E_{\mathrm{T}}^{d}\right| \ll k_{\mathrm{B}}T$ resulting in a strong mixing of the states due to thermal fluctuations.

Pure dephasing can originate from orbital effects. In our current description of the problem, we have neglected that the wave functions of the singlet $|\mathrm{S}(2,0)\rangle$ and triplet $|\mathrm{T}_+(1,1)\rangle$ couple differently to the background charge environment due to their different charge configurations. Thus, a superposition state of the form $|\psi\rangle = \alpha|\mathrm{S}(2,0)\rangle + \beta|\mathrm{T}_+(1,1)\rangle$ is sensitive to background charge fluctuations (charge noise), which leads to dephasing of the state $|\psi\rangle$[8,52]. If the qubit is in a superposition with the same charge state, $|\varphi\rangle = \alpha|\mathrm{S}(1,1)\rangle + \beta|\mathrm{T}_+(1,1)\rangle$, then the effects of charge noise are negligible. Therefore, the dephasing can be written as

$$\Gamma_\varphi(\varepsilon) = \gamma_2(1 - |c(\varepsilon)|^2), \tag{43}$$

where γ_2 is the charge noise rate. This form ensures that charge noise induced dephasing is suppressed when the spin states have the same charge configuration. In Fig. 5, we plot the rates $\Gamma_1(\varepsilon)$ and $\Gamma_\varphi(\varepsilon)$.

Finally, the Bloch equations, written in a matrix form, and describing the dynamics around the S-T$_+$ anti-crossing are

$$\hbar\begin{pmatrix}\dot{x}\\ \dot{y}\\ \dot{z}\end{pmatrix} = \begin{pmatrix} -\frac{1}{2}\hbar(\Gamma_1(\varepsilon(t)) + 4\Gamma_\varphi(\varepsilon(t))) & -E_{\mathrm{S}}(\varepsilon(t)) + \tilde{E}_{\mathrm{T}} & 0 \\ E_{\mathrm{S}}(\varepsilon(t)) - \tilde{E}_{\mathrm{T}} & -\frac{1}{2}\hbar(\Gamma_1(\varepsilon(t)) + 2\Gamma_\varphi(\varepsilon(t))) & -2\lambda c(\varepsilon(t)) \\ 0 & 2\lambda c(\varepsilon(t)) & -\hbar\Gamma_1(\varepsilon(t)) \end{pmatrix}\begin{pmatrix}x\\ y\\ z\end{pmatrix} \pm \hbar\begin{pmatrix}0\\ 0\\ \gamma_1\end{pmatrix}. \tag{44}$$

The different signs in front of the inhomogeneous term come from the fact that the states $|\mathrm{S}\rangle$ and $|\mathrm{T}\rangle$ exchange their roles as ground and excited state of the system at $\varepsilon = \varepsilon_{\mathrm{c}}$.

IV. RESULTS

We now compute the singlet return probability for two different detuning functions $\varepsilon(t)$. We first consider the case where $\varepsilon(t)$ is obtained through convolution of a trapezoid pulse with a Gaussian. We then consider what we call a "double hat" pulse [see Fig. 1(d)]. This is a pulse consisting of a fast-slow-fast rise-time succeeded by a waiting time and a reverse fast-slow-fast rise-time. Both types of detuning pulses have already been experimentally used to demonstrate control over a S - T$_+$ based qubit[16,18].

As stated previously, here we are interested in studying the effect of charge dynamics on the partial adiabatic spin dynamics in the vicinity of the hyperfine mediated anti-crossing. We therefore solve Eq. (44) for different values of γ_1 and γ_2. The singlet return probability is obtained by solving Eq. (44) for different realizations of λ that obey the probability distribution defined in Eq. (25). Since the actual number of nuclear spins interacting with the electron spin is unknown, we use the experimentally measured hyperfine splitting from Ref. 16 to determine the standard deviation. The average value of P_S is then calculated according to

$$P_\mathrm{S} = \frac{1}{N}\sum_{i=1}^{N}\frac{1}{2}\left(1 + z^{(i)}\right), \qquad (45)$$

where $z^{(i)}$ is the ith solution of $z(t)$ in Eq. (44).

A. Quantum Control with Convoluted Pulses

We start considering the case where $\varepsilon(t)$ is the result of the convolution between a square pulse with a rise-time of 1.5 ns, a variable width, and a maximal amplitude of 67.5 μeV, and a normalized Gaussian whose standard deviation is 3.7 ns [see Fig. 1(d)]. We plot in Fig. 6(a)-(d) the corresponding singlet return probability P_S as a function of t_w and nominal final position ε_f for different values of γ_1 and γ_2. We show in Fig. 6(e)-(f) traces taken at $\varepsilon_\mathrm{f} = 3.985\,\mathrm{meV}$ (before the anti-crossing) and $\varepsilon_\mathrm{f} = 3.95\,\mathrm{meV}$. Here, we have chosen $B = 100\,\mathrm{mT}$, $u = 4\,\mathrm{meV}$, $\tau = 5\,\mu\mathrm{eV}$ and respectively $\gamma_1 = 10^4\,\mathrm{s}^{-1}$, $\gamma_2 = 10^8\,\mathrm{s}^{-1}$ [(a), blue trace (e)-(f)], $\gamma_1 = 10^4\,\mathrm{s}^{-1}$, $\gamma_2 = 10^9\,\mathrm{s}^{-1}$ [(b), green trace (e)-(f)], $\gamma_1 = 10^5\,\mathrm{s}^{-1}$, $\gamma_2 = 10^8\,\mathrm{s}^{-1}$ [(c), purple trace (e)-(f)], $\gamma_1 = 10^5\,\mathrm{s}^{-1}$, $\gamma_2 = 10^9\,\mathrm{s}^{-1}$ [(d), red trace (e)-(f)]. Our results indicate that charge noise strongly affects the dynamics while spin relaxation only has a moderate effect. Although this behavior can be identified when comparing Fig. 6(a) with Fig. 6(b) and Fig. 6(c), it is best seen in Fig. 6(f) when comparing traces. An increase in the noise rate γ_2 leads to a substantial decrease of the oscillation visibility (blue and green traces). On the other hand, the visibility is only slightly diminished when relaxation is enhanced (blue and purple traces).

Here, charge noise has two important consequences on spin dynamics. We have already mentioned that it leads to dephasing of the qubit when its state is a superposition of spin and charge states. The second consequence is a mechanism which competes with the LZSM interferometry[53–56]. Since the hyperfine mediated anti-crossing is close to the charge anti-crossing for reasonable values of B, charge noise also affects the dynamics during the passage through the anti-crossing. As a result, the efficiency of the LZSM mechanism to create a coherent superposition or to produce coherent interferences is hindered, and thus the optimal states populations are not reached. This behavior can be identified in Fig. 6(f) when comparing traces obtained with same relaxation rate, but different charge noise rates (i.e. blue with green trace and purple with red trace). We clearly identify that the visibility of the oscillations is smaller for larger values of γ_2.

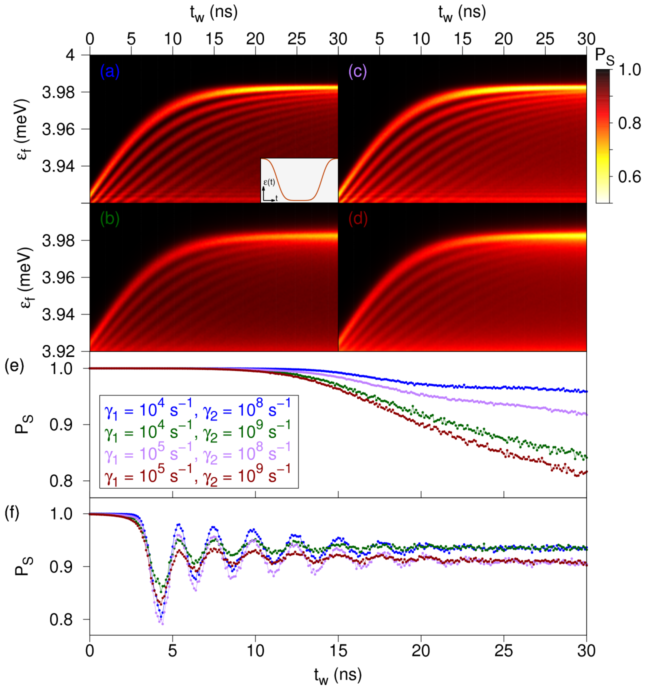

Figure 6. (color online) Singlet return probability P_S as a function of the waiting time t_w and final position ε_f obtained for a Gaussian detuning pulse. Here, we have set $B = 100\,\mathrm{mT}$, $u = 4\,\mathrm{meV}$, and $\tau = 5\,\mu\mathrm{eV}$ for all plots. The parameters γ_1 and γ_2 are (a) $\gamma_1 = 10^4\,\mathrm{s}^{-1}$, $\gamma_2 = 10^8\,\mathrm{s}^{-1}$, (b) $\gamma_1 = 10^4\,\mathrm{s}^{-1}$, $\gamma_2 = 10^9\,\mathrm{s}^{-1}$, (c) $\gamma_1 = 10^5\,\mathrm{s}^{-1}$, $\gamma_2 = 10^8\,\mathrm{s}^{-1}$, and (d) $\gamma_1 = 10^5\,\mathrm{s}^{-1}$, $\gamma_2 = 10^9\,\mathrm{s}^{-1}$. Figures (e) and (f) show cuts for case (a) in blue, (b) in green, (c) in purple, and (d) in red. The cuts are respectively taken before the anti-crossing at $\varepsilon_\mathrm{f} = 3.985\,\mathrm{meV}$ and after at $\varepsilon_\mathrm{f} = 3.95\,\mathrm{meV}$. These results show that charge noise is an important source of dephasing.

It is not ideal to use detuning pulses with rise-times that are long compared to the dephasing time set by charge noise. Although we have chosen a trapezoid pulse with a rise-time of 1.5 ns, the effective rise-time due to the convolution is $\approx$ 10 ns. Under such conditions, the charge noise induced spin decoherence mechanism dominates for $\varepsilon > \varepsilon_\mathrm{c}$. It thus becomes impossible to observe finite-time effects, as it can be seen in Fig. 6(e).

Energy relaxation processes have a weaker influence on spin dynamics than dephasing due to their dependence on the energy difference between the eigenstates of the system. These become only important when the system is held in close vicinity of the anti-crossing, where the relaxation rate is at its maximum [c.f. Fig. 5(a)].

B. Quantum Control with “Double Hat” Pulses

We now consider a “double hat” detuning pulse[18] [see Fig. 1(d)], whose leading and trailing edges are a sequence of fast-slow-fast rise-time pulses as described in Sec. II. This control method has the benefit of achieving a large adiabatic transition probability without exponentially extending the overall pulse length. In terms of qubit manipulation, this means larger amplitude rotations can be achieved in one passage.

We consider a detuning pulse $\varepsilon(t)$ with an amplitude of $\varepsilon_\mathrm{f} - \varepsilon_\mathrm{i} = 0.2\,\mathrm{meV}$. The pulse reaches an amplitude of $0.12\,\mathrm{meV}$ in $0.1\,\mathrm{ns}$, it is then slowed down until it reaches an amplitude of $0.1325\,\mathrm{meV}$, and finally it is brought to its maximal amplitude in $0.1\,\mathrm{ns}$. The rise time t_slow of the slow part of the pulse can be tuned freely. Here we compute P_S for $t_\mathrm{slow} = 6\,\mathrm{ns}$. In Fig. 7(a)-(d), we present the singlet return probability as a function of the final position ε_f and waiting time t_w for the same previously considered parameters. The interference fringes are characterized, for $\varepsilon < \varepsilon_\mathrm{c}$, by three distinct regions showing an alternate oscillation amplitude for P_S. The darker regions coincide with detunings for which the passage through the anti-crossing happened during one of the fast rise-times of $\varepsilon(t)$. Similarly, the bright region between $\varepsilon \simeq 3.900 - 3.915\,\mathrm{meV}$ coincides with a passage through the anti-crossing with the slow rise-time portion of the detuning pulse. This region exhibits better oscillation visibility than what is obtained with a Gaussian pulse. These results are consistent with previous experiments[18].

This type of detuning pulse allows the direct observation of finite-time effects in LZSM interferometry. We clearly identify coherent evolution of the qubit for $\varepsilon > \varepsilon_\mathrm{c}$, Fig. 7(e) [blue and purple trace, $\gamma_2 = 10^8\,\mathrm{s}^{-1}$]. This indicates that it is possible to design complex pulses that can directly influence the competition between LZSM physics and charge noise. However, this is conditional on the dephasing time scale associated with charge noise. We notice that if $\gamma_2 = 10^9\,\mathrm{s}^{-1}$, then it is impossible to identify any coherent behavior [green and red traces Fig. 7(e)]. These results suggest that inhomogeneous dephasing due to nuclear spin fluctuations is not the only physical process that limits the coherence of a two-spin based qubit, but also charge noise plays a major role. This is an important result for future devices made out of Si/SiGe which are reaching a maturity level comparable to GaAs[57,58]. Silicon based devices are very interesting candidates for spin based quantum computing because the only stable isotope (^{29}Si) possessing a nuclear spin ($I = 1/2$) has relatively low abundance, $\approx 5\%$. Thus, hyperfine induced decoherence is weaker than in GaAs based nanostructures[57].

Consequently, we distinguish three time scales that govern the physics of partial spin adiabatic passage in DQDs. There is the rise-time of the detuning pulse, the decoherence time T_2^*, and T_φ associated with charge noise induced dephasing. Ideally, we would like to have rise-times shorter than T_φ to preserve any spin superposition state. But this would render adiabatic transitions unlikely and therefore seriously hinder manipulation of the qubit. Double hat pulses partially solve the problem, but for an even better result, it would be necessary to increase the coupling between the qubit states. In GaAs double quantum dots, it is possible to prepare a nuclear gradient field to enhance the hyperfine coupling[14], with the advantage of extending T_2^*. In almost nuclear spin free systems (Si or C based DQDs), it is possible to use micro-magnets to artificially induce a coupling between the singlet state and triplet T_+[60].

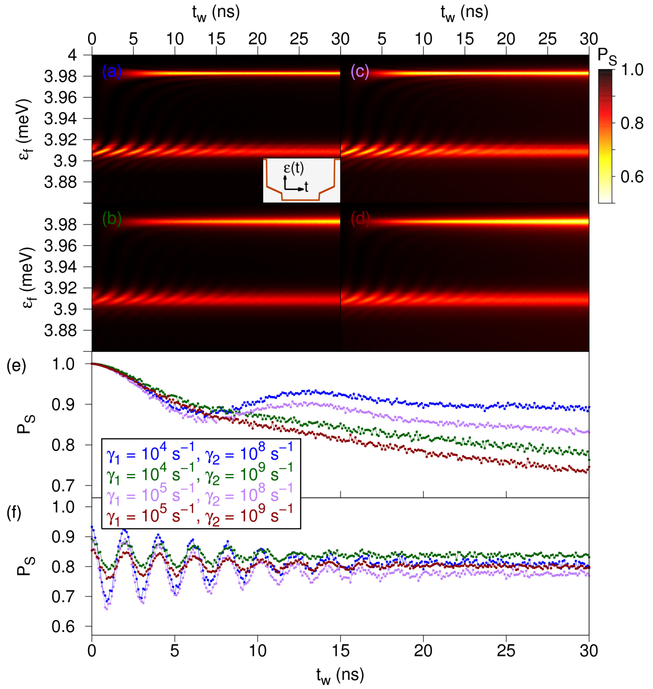

Figure 7. (color online) Singlet return probability P_S as a function of the waiting time t_w and final position ε_f obtained for a “double hat” detuning pulse. Pulse details are given in the text. Here, we have set $B = 100\,\mathrm{mT}$, $u = 4\,\mathrm{meV}$, and $\tau = 5\,\mu\mathrm{eV}$ for all plots. The parameters γ_1 and γ_2 are (a) $\gamma_1 = 10^4\,\mathrm{s}^{-1}$, $\gamma_2 = 10^8\,\mathrm{s}^{-1}$, (b) $\gamma_1 = 10^4\,\mathrm{s}^{-1}$, $\gamma_2 = 10^9\,\mathrm{s}^{-1}$, (c) $\gamma_1 = 10^5\,\mathrm{s}^{-1}$, $\gamma_2 = 10^8\,\mathrm{s}^{-1}$, and (d) $\gamma_1 = 10^5\,\mathrm{s}^{-1}$, $\gamma_2 = 10^9\,\mathrm{s}^{-1}$. Figures (e) and (f) show cuts for case (a) in blue, (b) in dark green, (c) in purple, and (d) in dark red. The cuts are respectively taken before the anti-crossing at $\varepsilon_\mathrm{f} = 3.985\,\mathrm{meV}$ and after at $\varepsilon_\mathrm{f} = 3.908\,\mathrm{meV}$.

C. Hadamard gate

We now demonstrate that charge induced spin dephasing is not a fundamental roadblock in the implementation

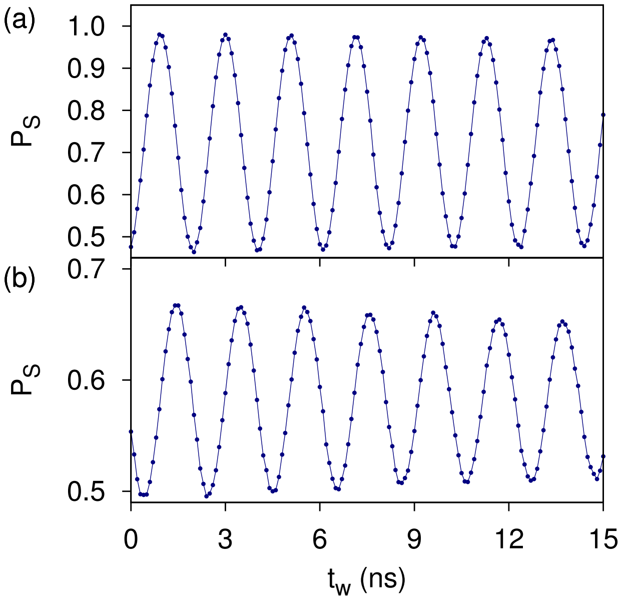

Figure 8. (color online) It is possible to achieve $P_{\mathrm{S}} = 0.5$ in the presence of charge dephasing by increasing the coupling between spin states to enhance the adiabatic transition probability. (a) Singlet state return probability for a prepared nuclear state with $t_{\mathrm{slow}} = 4\,\mathrm{ns}$, $\gamma_1 = 10^4\,\mathrm{s}^{-1}$, and $\gamma_2 = 10^8\,\mathrm{s}^{-1}$. (b) In case of fastest charge decoherence, it is still possible to achieve perfect beam splitting by further increasing the coupling. This is achieve by increasing $t_{\mathrm{slow}} = 8\,\mathrm{ns}$. We have $\gamma_1 = 10^4\,\mathrm{s}^{-1}$, and $\gamma_2 = 10^9\,\mathrm{s}^{-1}$.

of high fidelity quantum gates using LZSM interferometry. We specifically show that it is possible to achieve $P_{\mathrm{S}} = 0.5$, this particular value being a signature of a perfect 50 : 50 beam splitter. For quantum information processing, this allows a Hadamard gate Eq. (1), which is required to perform some quantum algorithms[27].

In the following, we consider a nuclear state that has been prepared according to the method developed in Ref. 14, i.e. a nuclear gradient field has been generated. We model such a prepared nuclear state by considering a mean difference field $\left|\delta\bar{B}_{\mathrm{n}}\right| = \left|\bar{B}_{\mathrm{n},2} - \bar{B}_{\mathrm{n},1}\right| = 10\,\mathrm{mT}$. The Gaussian distribution of nuclear fields Eq. (25) is changed to reproduce the mean $\delta\bar{B}_{\mathrm{n}}$. To take into account reduced nuclear fluctuations we consider a standard deviation $\sigma_{\mathrm{prep}} = \sigma/6$. We present in Fig. 8(a) a cut of the return singlet probability for a "double hat" pulse along $\varepsilon_{\mathrm{f}} = 3.911\,\mathrm{meV}$ with $t_{\mathrm{slow}} = 4\,\mathrm{ns}$, $B = 100\,\mathrm{mT}$, $u = 4\,\mathrm{meV}$, $\tau = 5\,\mu\mathrm{eV}$, $\gamma_1 = 10^4\,\mathrm{s}^{-1}$, and $\gamma_2 = 10^8\,\mathrm{s}^{-1}$. The results demonstrate that for this particular choice of parameters, it is possible to achieve $P_{\mathrm{S}} = 0.5$.

The remaining question is whether it is still possible to achieve $P_{\mathrm{S}} = 0.5$, if the charge noise rate γ_2 is increased. As expected from our previous analysis, and for the previous set of parameters, it is not possible. However, if we increase the coupling by increasing t_{slow}, we can again achieve perfect beam splitting. This is presented in Fig. 8 (b), where we have plotted a cut of the singlet return probability along $\varepsilon_{\mathrm{f}} = 3.9075\,\mathrm{meV}$ with $t_{\mathrm{slow}} = 8\,\mathrm{ns}$, $B = 100\,\mathrm{mT}$, $u = 4\,\mathrm{meV}$, $\tau = 5\,\mu\mathrm{eV}$, $\gamma_1 = 10^4\,\mathrm{s}^{-1}$, and $\gamma_2 = 10^9\,\mathrm{s}^{-1}$. Although these results demonstrate that in principle it is possible to reach $P_{\mathrm{S}} = 0.5$, it is still necessary to study the average gate fidelity. This goes beyond the scope of this paper and will be presented elsewhere.

V. CONCLUSIONS

We have developed a master equation formalism to study the dynamics of a S-T_+ qubit in the vicinity of the hyperfine mediated anti-crossing. In comparison with previous theories that only included decoherence due to nuclear spin fluctuation, we also include spin relaxation (e.g. due to spin-orbit) and spin dephasing due to charge dynamics phenomenologically. We have also derived a new effective two-level spin-charge Hamiltonian. In addition to previous theories, we take into account the charge degree of freedom. This property originates from the ground state singlet $|\mathrm{S}\rangle$ being a superposition of different charge configurations. Although the effective Hamiltonian is strictly not of the LZSM form, the peculiar form of the coupling constant allows to still reason in terms of LZSM physics.

Using our formalism, we have calculated the singlet return probability for two types of detuning pulses. For each case, we have compared results for different values of γ_1 and γ_2. Our findings suggest that LZSM spin interferometry can be inhibited by charge dynamics, and thus charge coherence has to be treated on equal footing with spin coherence. We have indeed demonstrated that the visibility of the spin qubit coherent oscillations is sensitive to the time scale associated with charge induced spin dephasing. We have also shown that this interplay between charge and spin can prevent the observation of finite-time oscillations. Interestingly, this last fact could lead to the development of a measurement protocol that would allow to quantify the time scale associated to charge decoherence.

Finally, we have demonstrated that in the case of a prepared nuclear state with a mean gradient field and a "double hat" detuning it is possible to achieve $P_{\mathrm{S}} = 0.5$. This demonstrates that an equally weighted superposition of S and T_+ can be reached. This is an important result for quantum information processings as it corresponds to the achievement of a Hadamard gate. It is an essential element in the implementation of important quantum algorithms like Shor's algorithm for period finding, and which ultimately allows to factorize large integers. Although we have supposed that a gradient field is created via the method developed in Ref. 14, it is possible to prepare the nuclear state via weak measurements as proposed in Ref. 49 to freeze the nuclear spin dynamics and create an artificial splitting by means of a micromagnet[60].

VI. ACKNOWLEDGEMENTS

HR and GB acknowledge funding from the DFG within SPP 1285 and SFB 767. Research at Princeton was supported by the Sloan and Packard Foundations and the National Science Foundation through the Princeton Center for Complex Materials, DMR-0819860 and CAREER award, DMR-0846341.

---

[1] D. Loss and D. P. DiVincenzo, Phys. Rev. A **57**, 120 (1998).

[2] R. Hanson, L. P. Kouwenhoven, J. R. Petta, S. Tarucha, L. M. K. Vandersypen, Rev. Mod. Phys. **79**, 1217 (2007).

[3] K. Ono, D. G. Austing, Y. Tokura, and S. Tarucha, Science **297**, 1313 (2002).

[4] M. Elzerman, R. Hanson, L. H. Willems van Beveren, B. Witkamp, L. M. K. Vandersypen, and L. P. Kouwenhoven, Nature **430**, 431 (2004).

[5] J. R. Petta, A. C. Johnson, J. M. Taylor, E. A. Laird, A. Yacoby, M. D. Lukin, C. M. Marcus, M. P. Hanson, and A. C. Gossard, Science **309**, 2180 (2005).

[6] F. H. L. Koppens, C. Buizert, K. J. Tielrooij, I. T. Vink, K. C. Nowack, T. Meunier, L. P. Kouwenhoven, and L. M. K. Vandersypen, Nature **442**, 766 (2006).

[7] K. C. Nowack, F. H. L. Koppens, Yu. V. Nazarov, and L. M. K. Vandersypen, Science **318**, 1430 (2007).

[8] W. A. Coish and D. Loss, Phys. Rev. B **72**, 125337 (2005).

[9] J. M. Taylor, J. R. Petta, A. C. Johnson, A. Yacoby, C. M. Marcus, and M. D. Lukin, Phys. Rev. B **76**, 035315 (2007).

[10] S. Nadj-Perge, S. M. Frolov, E. P. A. M. Bakkers, and L. P. Kouwenhoven, Nature **468**, 1084 (2010).

[11] J. Levy, Phys. Rev. Lett. **89**, 1147902 (2002).

[12] I. van Weperen, B. D. Armstrong, E. A. Laird, J. Medford, C. M. Marcus, M. P. Hanson, and A. C. Gossard, Phys. Rev. Lett. **107**, 030506 (2011).

[13] M. D. Shulman, O. E. Dial, S. P. Harvey, H. Bluhm, V. Umansky, A. Yacoby, Science, **336**, 202 (2012).

[14] S. Foletti, H. Bluhm, D. Mahalu, V. Umansky, and A. Yacoby, Nat. Phys. **5**, 903 (2009).

[15] A. V. Khaetskii, D. Loss, and L. Glazman, Phys. Rev. Lett. **88**, 186802 (2002).

[16] J. R. Petta, H. Lu, and A. C. Gossard, Science **327**, 669 (2010).

[17] H. Ribeiro, J. R. Petta, and G. Burkard, Phys. Rev. B **82**, 115445 (2010).

[18] H. Ribeiro, G. Burkard, J. R. Petta, H. Lu, and A. C. Gossard, arXiv:1207.2972.

[19] L. D. Landau, Phys. Z. Sowjetunion **2**, 46 (1932).

[20] C. Zener, Proc. R. Soc. A **137**, 696 (1932).

[21] E. C. G. Stückelberg, Helv. Phys. Acta **5**, 369 (1932).

[22] E. Majorana, Nuovo Cimento **9**, 43 (1932).

[23] S. N. Shevchenko, S. Ashhab, and F. Nori, Physics Reports **492**, 1-30 (2010).

[24] W. D. Oliver, Yang Yu, Janice C. Lee, Karl K. Berggren, Leonid S. Levitov, and Terry P. Orlando, Science **310**, 1653 (2005).

[25] T. Hayashi, T. Fujisawa, H. D. Cheong, Y. H. Jeong, and Y. Hirayama, Phys. Rev. Lett. **91**, 226804 (2003).

[26] J. R. Petta, A. C. Johnson, C. M. Marcus, M. P. Hanson, and A. C. Gossard, Phys. Rev. Lett. **93**, 186802 (2004).

[27] P. Shor, SIAM Journal of Computing **26**, 1484 (1997).

[28] I. I. Rabi, Phys. Rev. **51**, 652 (1937).

[29] R. Hanson and D. D. Awschalom, Nature **453**, 1043 (2008).

[30] A. Abragam, *Principles of Nuclear Magnetism*, Oxford University Press, New York, (1961).

[31] N. Rosen and C. Zener, Phys. Rev. **40**, 502 (1932).

[32] L. Allen and J. H. Eberly, *Optical Resonance and Two-Level Atoms*, (Dover, New York, 1987).

[33] F. T. Hioe, Phys. Rev. A **30**, 2100 (1984).

[34] A. Bambini and P. R. Berman, Phys. Rev. A **23**, 2496 (1981).

[35] Y. N. Demkov and M. Kunike, Vestn. Leningr. Univ. Fiz. Khim. **16**, 39 (1969).

[36] F. T. Hioe and C. E. Carroll, Phys. Rev. A **32**, 1541 (1985).

[37] J. Zakrzewski, Phys. Rev. A **32**, 3748 (1985).

[38] Y. N. Demkov, Sov. Phys.-JETP **18**, 138 (1964).

[39] E. E. Nikitin, Opt. Spectrosc. **13**, 431 (1962).

[40] C. E. Carroll and F. T. Hioe, J. Phys. A: Math. Gen. **19**, 3579 (1986).

[41] N. V. Vitanov, B. M. Garraway, Phys. Rev. A **53**, 4288 (1996).

[42] M. Abramowitz and I. A. Stegun, *Handbook of Mathematical Functions*, Ch. 6, Dover (1970).

[43] A. Erdélyi, W. Magnus, F. Oberhettinger, and F.G. Tricomi, *Higher Transcendental Functions*, Vol. II, Ch. 8, McGraw-Hill, New York, (1953).

[44] B. T. Torosov, S. Guérin, and N. V. Vitanov, Phys. Rev. Lett. **106**, 233001 (2011).

[45] H. Bluhm, S. Foletti, I. Neder, M. Rudner, D. Mahalu, V. Umansky, and A. Yacoby, Nat. Phys. **7**, 109 (2011).

[46] S. A. Studenikin, G. C. Aers, G. Granger, L. Gaudreau, A. Kam, P. Zawadzki, Z. R. Wasilewski, and A. S. Sachrajda, Phys. Rev. Lett. **108**, 226802 (2012).

[47] R. Hanson, L. M. K. Vandersypen, L. H. Willems van Beveren, J. M. Elzerman, I. T. Vink, and L. P. Kouwenhoven, Phys. Rev. B **70**, 241304(R) (2004).

[48] G. Burkard, D. Loss, and D. P. DiVincenzo, Phys. Rev. B **59**, 2070 (1999).

[49] H. Ribeiro and G. Burkard, Phys. Rev. Lett. **102**, 216802, (2009).

[50] G. Lindblad, Commun. Math. Phys. **48**, 119 (1976).

[51] H. P. Breuer and F. Petruccione, *Theory of open quantum systems*, Oxford University Press, (2007).

[52] X. Hu and S. Das Sarma, Phys. Rev. Lett. **96**, 100501 (2006).

[53] P. Ao and J. Rammer, Phys. Rev. Lett. **62**, 3004 (1989).

[54] E. Shimshoni and Y. Gefen, Ann. Phys. **210**, 16 (1991).

[55] P. Nalbach and M. Thorwart, Phys. Rev. Lett. **103**, 220401 (2009).

[56] P. P. Orth, A. Imambekov, K. Le Hur, Phys. Rev. A **82**, 032118 (2010).

[57] B. M. Maune, M. G. Borselli, B. Huang, T. D. Ladd, P. W. Deelman, K. S. Holabird, A. A. Kiselev, I. Alvarado-Rodriguez, R. S. Ross, A. E. Schmitz, M. Sokolich, C. A. Watson, M. F. Gyure, and A. T. Hunter, Nature **481**, 344 (2012).

[58] D. E. Savage, M. G. Lagally, L. R. Schreiber, L. M. K. Vandersypen, Mark Friesen, Robert Joynt, S. N. Coppersmith, and M. A. Eriksson, Phys. Rev. Lett. **108**, 046808 (2012).

[59] Y. Dovzhenko, J. Stehlik, K. D. Petersson, J. R. Petta, H. Lu, and A. C. Gossard, Phys. Rev. B **84**, 161302(R) (2011).

[60] M. Pioro-Ladrière, T. Obata, Y. Tokura, Y.-S. Shin, T. Kubo, K. Yoshida, T. Taniyama, and S. Tarucha, Nat. Phys. **4**, 776 (2008).